Journal of Zhejiang University-SCIENCE A 2026 27(1):12-25
www.jzus.zju.edu.cn; www.springer.com/journal/11582
E-mail: jzus_a@zju.edu.cn

Research Article
https://doi.org/10.1631/jzus.A2500019

Check for updates

Fast prediction of vibration source intensity induced by metro trains moving on regular and floating slab tracks

Lihui XU[1]✉, Meng GAO[1], Xinyu TAN[2], Chao ZOU[3], Meng MA[4]

[1]*College of Civil Engineering and Architecture, Shandong University of Science and Technology, Qingdao 266590, China*
[2]*National Engineering Research Center for Digital Construction and Evaluation Technology of Urban Rail Transit, China Railway Design Corporation, Tianjin 300308, China*
[3]*School of Civil and Transportation Engineering, Guangdong University of Technology, Guangzhou 510006, China*
[4]*Key Laboratory of Urban Underground Engineering of Ministry of Education, Beijing Jiaotong University, Beijing 100044, China*

Abstract: A complementary method to determine the vibration source intensity, defined as the weighted vertical acceleration level at the tunnel wall, is needed urgently when comparable measurements or database predictions are unavailable in empirical predictions. In this study, we present an analytical model designed to quickly and accurately estimate the vibration source intensity produced by moving metro trains, considering both regular and floating slab tracks. The improved periodic pipe-in-pipe (PiP) model with regular or floating slabs affixed to the tunnel invert was developed. The train loads are represented in the frequency-wavenumber domain to apply in the model. Measured track irregularities were applied and the proposed model was validated against the measured results and verified by a tunnel-soil coupled model. The proposed approach effectively and accurately assessed the vibration source intensity generated by underground trains in a prediction time of just 58 s. Track irregularities significantly affect the vibration source intensity, making them a key factor in comparable measurements or database predictions. A floating slab track can reduce the vibration source intensity by about 14 dB. The proposed approach can serve as an additional method to complement comparable measurements or database predictions for determining the vibration source intensity in empirical predictions.

Key words: Environmental vibration prediction; Vibration source intensity; Analytical prediction model; Floating slab track; Measured track irregularities

1 Introduction

The vigorous expansion of metro lines has raised significant environmental concerns due to the adverse effects of induced vibrations on nearby historical buildings, residential housing, and precision instruments (Kouroussis et al., 2018; Sheng, 2019; Xu and Ma, 2024; Li and Ma, 2025). The first step in designing environmental vibration control measures is typically to accurately predict the vibrations of the ground and buildings. During the early phase of metro tunnel construction, empirical prediction methods are commonly used to swiftly assess vibration levels at sensitive locations along the entire metro route, with the vibration source intensity VL_{z0} (in dB) established based on measurements from similar sections elsewhere or a database. The vibration source intensity VL_{z0} is defined as the weighted vertical acceleration level at the tunnel wall and is calculated as $VL_{z0}=20\lg(a_{rms,w}/a_0)$ (where $a_{rms,w}$ is the root mean square (RMS) of weighted accelerations and $a_0=1\times10^{-6}$ m/s^2 is the reference acceleration). There is an urgent need for a supplementary method to predict the vibration source intensity quickly and accurately in the absence of analogous tunnel sections for comparable measurements or database predictions. In this study, we aimed to develop an analytical model that can rapidly and accurately predict the vibration source intensity generated by moving metro trains, considering both regular and floating slab tracks.

Vibration prediction is crucial for optimising routes and managing vibrations effectively. Different methods have been proposed to predict vibrations from underground sources, including semi-analytical/analytical models (Yuan et al., 2017, 2021; He et al., 2018, 2024;

✉ Lihui XU, xlh@sdust.edu.cn
Lihui XU, https://orcid.org/0000-0001-8003-4259

Received Jan. 20, 2025; Revision accepted Apr. 17, 2025;
Crosschecked Sept. 23, 2025; Online first Dec. 22, 2025

Xu and Ma, 2023; Ma et al., 2024), numerical models (François et al., 2010; Vogiatzis and Kouroussis, 2015; Liravi et al., 2022; Liu et al., 2023; Azhir et al., 2024; Di et al., 2024), hybrid models (Verbraken et al., 2013; Kouroussis et al., 2018; Colaço et al., 2022; Dai et al., 2024), and empirical models (Banestyrelsen, 2000; ISO, 2005; Koopman et al., 2009; BMBMSA, 2019). Typically, the empirical models, namely chain-type formulas, are applied to identify locations with excessive vibrations. Kurzweil (1979) first proposed an empirical model by decoupling the system into three parts: the vibration source, the transmission path, and the receiver. This model has since been further refined by various researchers, including Melke (1988) and Madshus et al. (1996). For its feasibility, chain-type empirical models have been endorsed by many technical codes across different countries, such as China (MEE, 2018) and the USA (USDT, 2018). According to the Chinese code (MEE, 2018), the environmental vibration level VL_z can be estimated using the empirical formula $VL_z=VL_{z0}+C_{VB}$, where C_{VB} is a correction item related to many factors, such as the train speed, tunnel configuration, soil parameters, and building parameters. The vibration source intensity is the core for vibration predictions and is determined from comparable measurements (MEE, 2018) or a database (BMBMSA, 2019; Xu et al., 2022). However, if the measurement conditions, such as track irregularities, differ from those of the target section, the result may be inaccurate.

The vibration source intensity and other characteristics like frequency content may vary depending on factors such as track irregularities, wheel unevenness, and train speed. In a one-day vibration monitoring study, Li et al. (2020) discovered that wheel unevenness can lead to a 20-dB change in vibrations within 8–200 Hz. Ma et al. (2021b, 2022) concluded that rail grinding and wheel profiling would reduce the source intensity by 10 and 8 dB, respectively. He et al. (2023) conducted an in-site measurement and found that track irregularities and wheel unevenness had a significant impact on the source intensity. From a statistical survey, Li et al. (2012) highlighted that the variation of source intensity in Beijing could reach up to 7 dB. Lu et al. (2010) found from a comparison measurement that the source intensity increased by 2 dB with every 5 km/h increase in train speed. Hence, discrepancies in train, track, and soil conditions may result in prediction errors when using comparable measurements (MEE, 2018) or database predictions (BMBMSA, 2019; Xu et al., 2022). These methods also do not sufficiently account for the track irregularity levels. Furthermore, in certain situations, there are no comparable tunnel sections available for conducting in-site measurements or for selecting the source intensity from a database. In this case, the numerical model used by Qu et al. (2023), which incorporates measured track irregularities and wheel unevenness as inputs, could serve as a substitute for determining the source intensity in the empirical model. However, numerical models require more time than comparable measurements or database predictions.

The pipe-in-pipe (PiP) model proposed by Forrest and Hunt (2006) can be applied to determine the dynamic response at the tunnel wall. In this model, the tunnel is conceptualized as an infinitely long shell and the surrounding soil is modeled as a continuum medium in a full space. The PiP model is advantageous due to its low memory usage and short computation time. Subsequently, this model was expanded to encompass various scenarios, including a multilayered halfspace (Hussein et al., 2008, 2014), floating slab track (Hussein and Hunt, 2009), twin tunnel (Kuo et al., 2011), poroelastic halfspace (Di et al., 2018), periodic jointed tunnel (He et al., 2019), and source-receiver interaction (Edirisinghe and Talbot, 2021). The accuracy and efficiency were validated through comparisons with the finite element-boundary element coupled model (Gupta et al., 2007). Recently, Yang et al. (2024) developed a train-track-circular tunnel spatially coupled model in which the surrounding soil was represented by a cylindrical viscoelastic layer. The tunnel-soil coupled system can be regarded as a periodic system because of the periodic arrangement of the discretely distributed fasteners (Ma et al., 2024). However, this type of periodicity has not yet been incorporated into the PiP model for assessing the vibration source intensity.

As noted above, when comparable measurements or database predictions are not feasible, there is a pressing need for an alternative method to accurately and swiftly predict the vibration source intensity generated by moving trains, in which the track irregularities should be sufficiently considered. The PiP model is suitable for this situation because of its low memory requirements and short computation time. However, the periodicity resulting from the discretely distributed fasteners has not yet been considered in the PiP model.

This study aimed to develop an analytical model to predict the vibration source intensity caused by moving metro trains quickly and accurately, considering both regular and floating slab tracks. The contributions of this work include: (1) offering an alternative to comparable measurements or database predictions considering the track irregularities, and (2) addressing the periodicity issue in the PiP model resulting from discretely distributed fasteners. First, the PiP model is extended to account for the periodicity arising from the discretely distributed fasteners. Then, both regular and floating slab tracks are modeled and integrated with the periodic PiP model. Next, the train load expression in the frequency-wavenumber domain is formulated. Measured track irregularities are applied in the prediction. The dynamic responses at the tunnel wall are examined for a regular slab track, with an exploration of the impacts of train speed, track irregularities, and surrounding soil. The isolation effects of a floating slab track are also revealed. Finally, some conclusions are drawn from the analyses.

2 Analytical prediction model for vibration source intensity

2.1 Model overview

Fig. 1 presents an overview of the train-track-tunnel-soil system, featuring both regular and floating slab tracks. In the calculations, the whole system is divided into two subsystems: the train-track subsystem and the track–tunnel–soil subsystem. The coupling of the above subsystems is accomplished by the transmission of supporting forces, which refer to the forces transmitted through fasteners from the rails to either the roadbed slab or the floating slab. The train–track subsystem modeled by Ma (2014) is summarized in the electronic supplementary materials (ESM).

In a track–tunnel–soil subsystem with a regular slab track, the supporting forces are discretely distributed on the track slab with a spacing of L=0.6 m, corresponding to the spacing of fasteners or sleepers. Ma (2014) showed that the forces of fasteners adhere to a periodicity relationship, resulting in the periodic nature

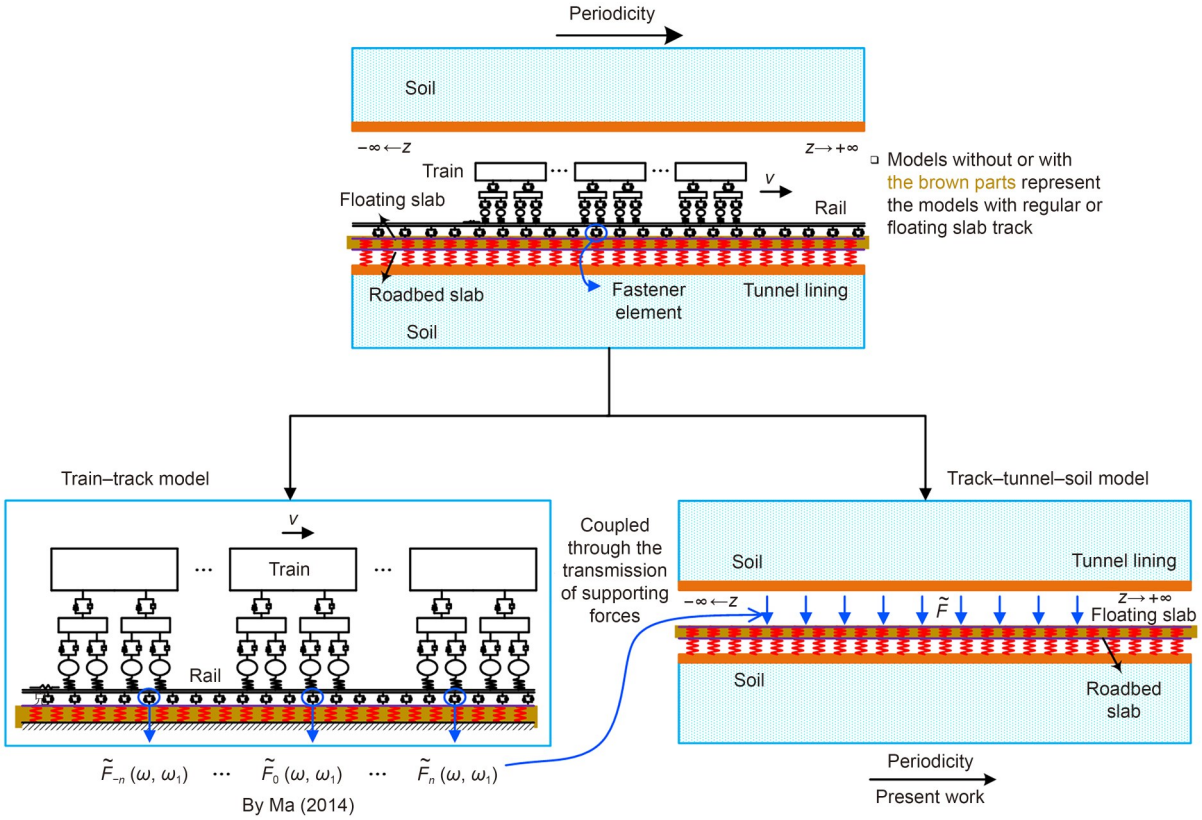

Fig. 1 Overview of the train–track–tunnel–soil system with a regular or floating slab track. $\tilde{F}_{-n}(\omega, \omega_1)$, $\tilde{F}_0(\omega, \omega_1)$, and $\tilde{F}_n(\omega, \omega_1)$ are the supporting forces, ω is the response frequency, and ω_1 is the excitation frequency. References to color refer to the online version of this figure

of the subsystem. Although the floating slab is constructed in a discontinuous manner, the presence of shear hinges between adjacent slabs allows it to be treated as a continuous slab, as illustrated in Fig. 1. Therefore, a similar periodicity exists. In both cases, the tunnel-soil system is modeled by the periodic PiP model. Both the roadbed slab and the floating slab are modeled as Euler beams. The interactions between the components are facilitated by continuous springs. Rails are excluded in this subsystem.

2.2 Periodic PiP model

Fig. 2 shows a schematic diagram of the periodic PiP model. The tunnel lining is represented as an infinitely long Flügge circular shell (r=R, r is the radial coordinate and R is the radius) (Flügge, 1973), while the surrounding soil is modeled as a continuum medium in a full space with a hollow ($r_s \in [R, \infty)$, r_s is the radial coordinate in the soil). We assumed that the presence of a free surface on the ground has no impact on the responses of the tunnel. This assumption was first adopted by Hussein et al. (2014) to predict the ground surface response, and good results were obtained. The forces from the roadbed slab beam are conveyed to the tunnel invert through the springs. The PiP model by Forrest and Hunt (2006) is expanded into a periodic PiP model, considering the periodicity of the supporting forces.

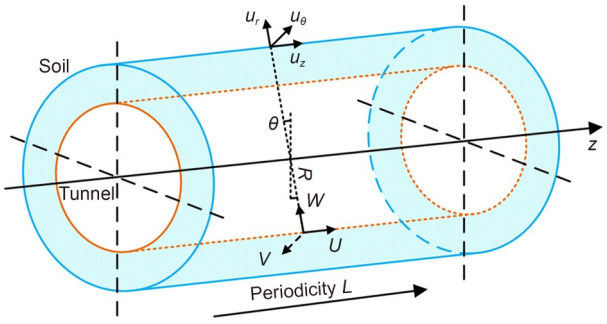

Fig. 2 Schematic diagram of the periodic PiP model. u_r, u_θ, and u_z denote the radial, circumferential, and longitudinal displacements of the soil while W, V, and U represent those of the tunnel, respectively. θ is the circumferential coordinate

Considering a moving periodic load with a periodicity length of L in the z direction, a frequency of ω_1, and a speed of v, the responses $\tilde{\Theta}(z,\omega,\omega_1)$ in the frequency domain can be represented as a summation of the generalized modal functions:

$$\tilde{\Theta}(z,\omega,\omega_1)=\sum_{n=-\infty}^{n=+\infty}\tilde{\Theta}_n(\omega)\Phi_n(z,\omega_1,\omega), \tag{1}$$

where $\Phi_n(z,\omega_1,\omega)=e^{i\lambda_n z}$ is the generalized modal function, and $\lambda_n=\frac{2\pi n}{L}+\frac{\omega_1-\omega}{v}$. $\tilde{\Theta}_n(\omega)$ represents the modal coefficients, n is the wavenumber, and the symbol ~ represents the quantity in the frequency domain.

Based on the Flügge shell theory, the relationship between displacements and tractions in the frequency-wavenumber domain can be derived:

$$\boldsymbol{A}_{\mathrm{E}}\tilde{\boldsymbol{U}}_{nm}=\tilde{\boldsymbol{Q}}_{nm}, \tag{2}$$

where $\tilde{\boldsymbol{U}}_{nm}$ and $\tilde{\boldsymbol{Q}}_{nm}$ are the tunnel displacement and traction vector (please refer to Eq. (S3) in the ESM). The subscript m represents the trigonometric series order. $\boldsymbol{A}_{\mathrm{E}}$ is a 3×3 coefficient matrix. Its elements are derived by Forrest and Hunt (2006), where the wavenumber ξ in the original expressions should be replaced by λ_n for a periodicity sense.

Solving the elastodynamic equations of the soil medium, the general solutions of soil displacements and stresses in the cylindrical coordinate can be formulated in the frequency-wavenumber domain (Xu and Ma, 2023). Only outgoing cylindrical waves exist in the full space of soil. The displacements $\tilde{\boldsymbol{u}}_{nm}$ and stresses $\tilde{\boldsymbol{t}}_{nm}$ at the interface r=R have the expressions:

$$\tilde{\boldsymbol{u}}_{nm}=\{\tilde{u}_{znm}\ \tilde{u}_{\theta nm}\ -\tilde{u}_{rnm}\}=\boldsymbol{\chi}_{\mathrm{o}}(r=R)\,\boldsymbol{B}_{\mathrm{o}nm}, \tag{3}$$

$$\tilde{\boldsymbol{t}}_{nm}=\{-\sigma_{rznm}\ -\sigma_{r\theta nm}\ \sigma_{rrnm}\}=\boldsymbol{\eta}_{\mathrm{o}}(r=R)\,\boldsymbol{B}_{\mathrm{o}nm}, \tag{4}$$

where the expressions of $\boldsymbol{\chi}_{\mathrm{o}}(r)$ and $\boldsymbol{\eta}_{\mathrm{o}}(r)$ are listed in the ESM. The subscript o represents the outgoing wave and $\boldsymbol{B}_{\mathrm{o}nm}$ is the unknown coefficient vector. The negative sign in the expressions is to keep the displacement and stress directions of soil consistent with those of the shell.

Considering the displacement compatibility and stress equilibrium, the tunnel displacement vector $\tilde{\boldsymbol{U}}_{nm}$ and soil known coefficient vector $\boldsymbol{B}_{\mathrm{o}nm}$ should satisfy the following equation:

$$\boldsymbol{K}_{nm}\tilde{\boldsymbol{U}}^{B}_{nm}=\begin{bmatrix}\boldsymbol{A}_{\mathrm{E}} & \boldsymbol{\eta}_{\mathrm{o}}(r=R)\\ \boldsymbol{I} & -\boldsymbol{\chi}_{\mathrm{o}}(r=R)\end{bmatrix}\begin{Bmatrix}\tilde{\boldsymbol{U}}_{nm}\\ \boldsymbol{B}_{\mathrm{o}nm}\end{Bmatrix}=\tilde{\boldsymbol{P}}^{0}_{nm}, \tag{5}$$

where $\boldsymbol{I}$ is the 3×3 unit matrix, $\tilde{\boldsymbol{P}}_{nm}^{0}=\{\tilde{\boldsymbol{P}}_{nm}\ 0\}^{\mathrm{T}}$, and $\tilde{\boldsymbol{P}}_{nm}$ is the load vector. $\boldsymbol{K}_{nm}=\begin{bmatrix}\boldsymbol{A}_{\mathrm{E}} & \boldsymbol{\eta}_{\mathrm{o}}(r=R)\\ \boldsymbol{I} & -\boldsymbol{\chi}_{\mathrm{o}}(r=R)\end{bmatrix}$ and $\tilde{\boldsymbol{U}}_{nm}^{B}=\begin{Bmatrix}\tilde{\boldsymbol{U}}_{nm}\\ \boldsymbol{B}_{onm}\end{Bmatrix}$.

After solving Eq. (5), the tunnel displacement $\tilde{\boldsymbol{U}}_{nm}$ can be obtained. Thus, the PiP model has been developed into the periodic PiP model using the principles of periodicity theory.

2.3 Analytical solution of the regular slab

In this study, the regular track slab is simplified as an infinitely long Euler beam attached to the tunnel invert via the continuously distributed springs along the longitudinal direction in the periodic PiP model (Fig. 3). The slab beam is subjected to supporting forces from moving trains.

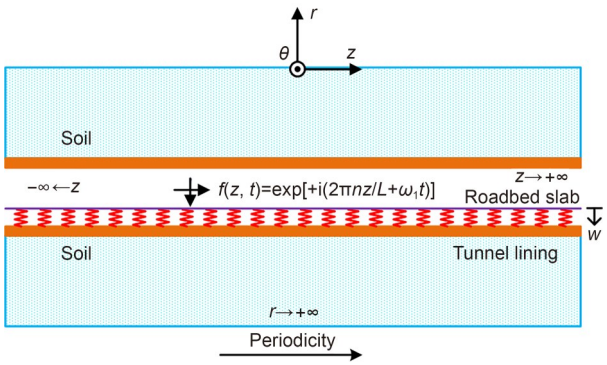

Fig. 3 Regular track slab attached to the tunnel invert in the periodic PiP model

Assuming a periodic load $f(z, t)$ with a periodicity length L, a frequency ω_1, and a wavenumber n moving on the slab beam at a speed of v, the motion equation of the beam is given by

$$m_{\mathrm{s}}\frac{\partial^2 w}{\partial t^2}+EI\frac{\partial^4 w}{\partial z^4}+(w+W^{\dagger})k_{\mathrm{eff}}=f(z,\ t),\quad (6)$$

where w is the displacement of the roadbed slab beam, m_{s} is the mass per unit length, and EI is the bending stiffness. $W^{\dagger}$ is the radial displacement at the tunnel invert (r=R, θ=π), and k_{eff} represents the effective stiffness of the equivalent spring that simulates the contacts between the roadbed and the tunnel invert.

Solving Eq. (6), the solution is derived as

$$\tilde{w}_n=\alpha\tilde{W}_n^{\dagger}+\tilde{\Delta}_n,\quad (7)$$

where $\alpha=-k_{\mathrm{eff}}/D$ and $\tilde{\Delta}_n=\tilde{f}_n/D$. The variable D has the expression $D=EI\lambda_n^4-m_{\mathrm{s}}\omega^2+k_{\mathrm{eff}}$ and $\tilde{f}_n$ denotes the load in the frequency-wavenumber domain. The expression for a moving periodic load is given by Xu and Ma (2023). The expression for a moving train load will be provided later.

According to the radial forces acting on the tunnel invert transmitted by the spring, the forces $\tilde{\boldsymbol{P}}_{nm}^{0}$ for each m can be obtained, as presented in the ESM. Substituting $\tilde{\boldsymbol{P}}_{nm}^{0}$ into Eq. (5) and considering m=0, 1, ⋯, M (M=8 is the truncation number of m), the equilibrium equations for the periodic PiP model with the regular track slab are derived:

$$(\boldsymbol{K}_n+k_{\mathrm{eff}}(1+\alpha)\boldsymbol{VC})\tilde{\boldsymbol{U}}_n^{B}=-k_{\mathrm{eff}}\tilde{\Delta}_n\boldsymbol{V},\quad (8)$$

where the matrices $\boldsymbol{K}_n$, $\boldsymbol{V}$, and $\boldsymbol{C}$ are given explicitly in the ESM.

There are 6(M+1) equilibrium equations in Eq. (8) to uniquely determine the known vector $\tilde{\boldsymbol{U}}_n^{B}$. Considering each wavenumber n and response frequency ω, the displacements of the tunnel and soil in the time-space domain are calculated. The value of M will affect both the accuracy and efficiency of the predictions. When M is set to 8, the prediction results reach convergence.

2.4 Analytical solution of the floating slab

As stated above, the floating slab was treated as a continuous slab in this study and modeled as an infinitely long Euler beam (Fig. 4). Note that the rubber pad beneath the floating slab is represented as a continuous spring. Additionally, the discrete supports of the floating slab can be simplified as a continuous spring.

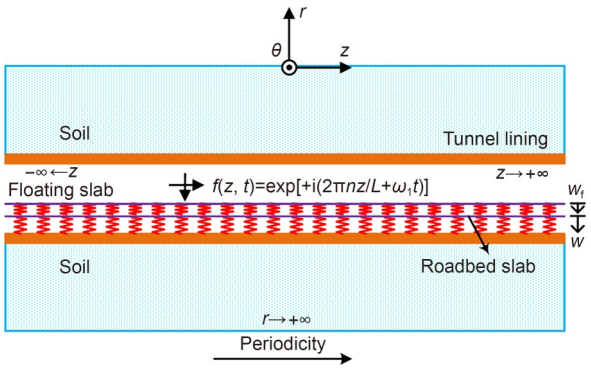

Fig. 4 Floating slab track attached to the tunnel invert in the periodic PiP model

Similarly, the equilibrium equations for the roadbed and floating slab beams have the forms

$$m_{\mathrm{s}}\frac{\partial^2 w}{\partial t^2}+EI\frac{\partial^4 w}{\partial z^4}+k_{\mathrm{eff}}(w+W^{\dagger})+k_{\mathrm{f}}(w-w_{\mathrm{f}})=0, \quad (9)$$

$$m_{\mathrm{f}}\frac{\partial^2 w_{\mathrm{f}}}{\partial t^2}+EI_{\mathrm{f}}\frac{\partial^4 w_{\mathrm{f}}}{\partial z^4}+k_{\mathrm{f}}(w_{\mathrm{f}}-w)=f(z,t), \quad (10)$$

where the subscript f represents the quantity for the floating slab.

Solving Eqs. (9) and (10), the following equation is derived:

$$\tilde{w}_n=\tilde{W}_n^{\dagger}\alpha^{*}+\tilde{\Delta}_n^{*}. \quad (11)$$

The expressions of α^{*} and $\tilde{\Delta}_n^{*}$ are given in the ESM.

By replacing α and $\tilde{\Delta}_n$ in Eq. (8) by α^{*} and $\tilde{\Delta}_n^{*}$ in Eq. (11), the model with the floating slab track can be established.

2.5 Train load expression in the frequency-wavenumber domain

As stated above, the supporting forces, specifically the train loads in this study, are applied discretely to both the regular track slab and the floating slab, each featuring a periodicity length of L=0.6 m (Fig. 5). The supporting forces are determined using the analytical model for periodic train-track and train-floating slab track interactions developed by Ma (2014). In the floating slab track model, the floating slab is treated as an infinitely long beam, and the discrete supports beneath the slab are approximated as a continuous spring.

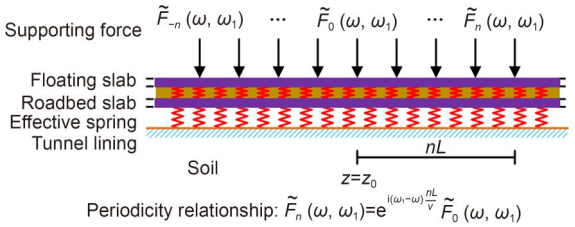

Fig. 5 Supporting forces periodically exerted on the regular track slab (without the brown parts) or floating slab. References to color refer to the online version of this figure

Ma (2014) showed that supporting forces $\tilde{F}_0(\omega,\omega_1)$ and $\tilde{F}_n(\omega,\omega_1)$ at z=z_0 and z=z_0+nL follow the periodicity relationship (Fig. 5). The total forces $\tilde{f}(z,\omega,\omega_1)$ acting on the slab are the sum of the supporting forces $\tilde{F}_n(\omega,\omega_1)$. By applying the periodicity feature and the discrete Fourier transform, the expression for the modal components $\tilde{f}_n(\omega,\omega_1)$ of $\tilde{f}(z,\omega,\omega_1)$ is given by

$$\tilde{f}_n(\omega,\omega_1)=\frac{\tilde{F}_0(\omega,\omega_1)}{L}\mathrm{e}^{-\mathrm{i}\left(\frac{2\pi n}{L}+\frac{\omega_1-\omega}{v}\right)z_0}. \quad (12)$$

Substituting Eq. (12) into Eqs. (7) and (11), the dynamic response of the tunnel lining and soil can be predicted quickly by Eq. (8). Note that the calculation should be repeated with respect to n, ω, and ω_1. To further enhance the prediction efficiency, two measures of the calculation efficiency improvement can be applied to reduce the calculation loops (Ma et al., 2024).

More detailed derivations are given in the ESM.

3 Model validation and verification

In this section, we present the validation of the proposed model against measured results with regular slab tracks in Beijing and verification against theoretical results.

3.1 Model parameter

The fastener supporting forces from metro trains were calculated using the analytical models (Ma, 2014). The parameters for the train, rails, and fasteners are listed in the ESM. The parameters for the roadbed slab and floating slab for the vibration source intensity predictions are listed in Table 1. Considering the damping effects, expressions $\bar{k}_{\mathrm{eff}}=k_{\mathrm{eff}}(1+\mathrm{i}\xi_{\mathrm{eff}})$ and $\bar{k}_{\mathrm{f}}=k_{\mathrm{f}}+\mathrm{i}\omega c_{\mathrm{f}}$ were applied to the roadbed and floating slab beams, respectively. In the predictions, three train speeds were considered: v=60, 70, and 80 km/h, corresponding to the maximum operation speed in Beijing.

Table 1 Mechanical parameters for the roadbed slab and floating slab

Roadbed slab		Floating slab	
Parameter	Value	Parameter	Value
EI (Pa·m^4)	1.43×10^9	EI_{f} (Pa·m^4)	4.1354×10^8
m_{s} (kg/m)	3500	m_{f} (kg/m)	2500
k_{eff} (N/m^2)	8.212×10^8	k_{f} (N/m^2)	7.36×10^6
ξ_{eff}	0.0643	c_{f} (N·s/m^2)	1.6×10^4

The soil parameters were sourced specifically from Beijing. Based on a statistical survey (Xu and Ma, 2020), the burial depth for metro tunnels in Beijing

ranges from 14 to 22 m. Within this depth range, the velocities of the compressional (c_p) and shear (c_s) waves traversing the soil were measured to be 470–610 and 225–293 m/s, respectively. The lower and upper bounds of these wave velocities were designated as S1 and S2, respectively, to model the surrounding soil in the subsequent analyses. The tunnel lining features a radius of 3 m and a thickness of 0.3 m. The parameters for the soil and tunnel lining are listed in Table 2.

Table 2 Parameters for the soil and tunnel lining

Material	Elastic modulus (MPa)	Poisson's ratio	Density (kg/m^3)	Damping
Soil-S1	230	0.375	1900	0.04
Soil-S2	475	0.300	1900	0.04
Lining concrete	32000	0.200	2400	0.01

3.2 Track irregularity

Track irregularities have significant effects on vibration predictions. Chen (2020) and Ma et al. (2021a) conducted a statistical survey of 439 sets of measured track irregularities from the Beijing metro and proposed a spectrum of Beijing track irregularities categorized into five classes, labeled Q1 to Q5. Classes Q1 and Q5, which represent tracks in extremely good and poor conditions, respectively, within the wavenumber range considered, are impossible in practical engineering. In most cases, classes Q2, Q3, and Q4 can effectively represent the track conditions (Ma et al., 2021a). For upper and lower limit analyses, only classes Q2 and Q4 were considered, representing the irregularity power spectrum density (PSD) at the 25th and 75th percentiles, respectively. The track irregularity PSD spectrum $S(\Omega)$ takes the following form when the wavenumber falls within the range of $1\times2\pi$ rad/m$<\Omega<100\times2\pi$ rad/m:

$$S(\Omega)=\begin{cases}A_1\Omega^{k_1}, & 1\times2\pi\ \text{rad/m}\leqslant\Omega<3\times2\pi\ \text{rad/m},\\ A_2\Omega^{k_2}, & 3\times2\pi\ \text{rad/m}\leqslant\Omega\leqslant100\times2\pi\ \text{rad/m}.\end{cases}\tag{13}$$

The parameters in Eq. (13) are listed in Table 3 for Q2 and Q4. In this study, short-wavelength irregularities with $\Omega>1\times2\pi$ rad/m were characterized by the Beijing spectrum, while long-wavelength irregularities with $\Omega<1\times2\pi$ rad/m were represented by the American spectrum, e.g., Q2+America class 5 (labeled Q2) or Q4+America class 1 (labeled Q4). In the frequency range of interest (0–100 Hz), when the train speed is 60–80 km/h, the relevant wavenumber Ω is less than 37.7 rad/m according to the relationship $\Omega=\omega/v$.

Table 3 Parameters for Beijing spectrum

Class	A_1	k_1	A_2	k_2
Q2	7.535	−4.301	0.0784	−2.746
Q4	79.620	−4.424	0.6490	−2.787

Fig. 6 shows a plot of classes Q2 and Q4 of the Beijing track irregularity PSD spectrum, with classes 1 and 6 of the American spectrums (US1 and US6) overlaid on the same figure. The trend of short-wavelength irregularities in the Beijing spectrum, especially $\Omega>3\times2\pi$ rad/m, differs from that in the American spectrum. This will affect the vibration within the frequency range of 16.7–100 Hz. To achieve a more accurate prediction, the wheel unevenness should be incorporated into the model.

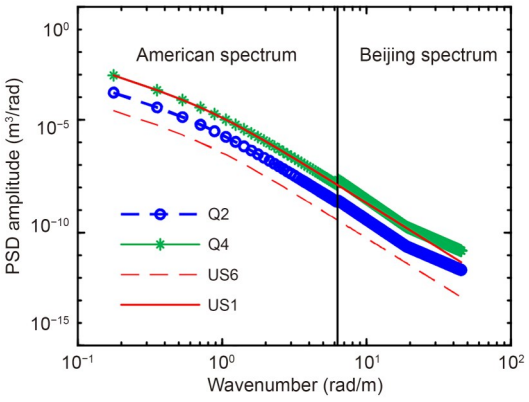

Fig. 6 Beijing track irregularity PSD spectrum for Q2 and Q4, overlaid with the American track spectrum (US1 and US6)

3.3 Validation

Validation was performed using the measured vibration source intensity at 11 tunnel locations within the Beijing metro. These sections feature a circular and straight tunnel that uses a regular-slab unique-centered track system with DTVI$_2$ fasteners. Trains with six carriages pass by these sections at speeds in the range of 60–80 km/h. Vertical vibrations at the tunnel wall were recorded by an accelerometer with a measurement range of 3g and a resolution of 0.02 mg. The accelerometer was positioned at a height of 1.5 m from the track bed according to the Chinese code (MEE, 2018) (Fig. 7). The measured vibration source intensities are presented in the ESM.

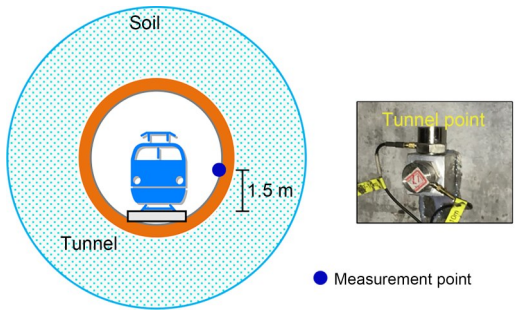

Fig. 7 Measurement point at the tunnel wall

In the predictions, soil types S1 and S2 were used to simulate the surrounding soil, while spectrums Q2 and Q4 were used, respectively, to represent the good and bad operational states of the track. Fig. 8 presents a comparison of the predicted vibration source intensities with the measured results. When the surrounding soil was classified as S2, which has higher wave velocities, the predicted results for Q2 and Q4 encompass most of the measured results. When the soil was classified as S1, the results are a little overestimated. On the other hand, when the track irregularities were classified as Q2 or Q4, changes in soil conditions did not lead to favorable outcomes, especially under Q4, which largely overestimated the vibration source intensity. Consequently, if the track irregularities used differ from the actual conditions of the track, the predictions will be inaccurate. In the environmental assessment, it is advisable to use the measured track irregularities to ascertain the vibration source intensity.

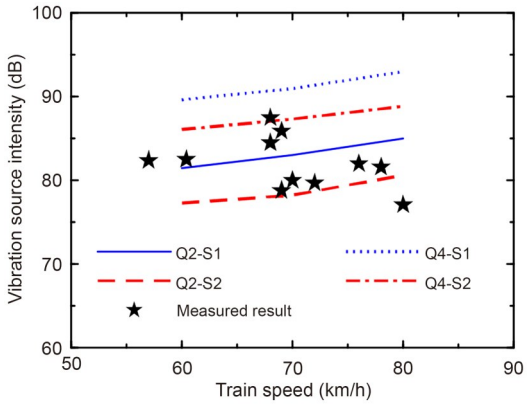

Fig. 8 Comparison of predicted vibration source intensity with measured results

Overall, the prediction provides both lower and upper bounds for the vibration source intensity generated by metro trains, demonstrating that the proposed model is accurate and reliable for determining the vibration source intensity in the empirical predictions.

3.4 Verification

The verified tunnel-soil analytical model (reference model, RM) established by Ma et al. (2024) was applied to verify the correctness of the present model (PM). The results for v=60 km/h, S1, and Q2 of the two models are presented in Fig. 9, showing the outcomes in the time domain, frequency domain, and one-third octave band.

The time history and frequency spectrum shown in Figs. 9a and 9b indicate that the waveforms produced by the current model closely resemble those of the reference model. In the one-third octave band from Fig. 9c, the discrepancies between these two models are below 3 dB, except for 1.25 Hz, where the discrepancy is about 5 dB. At the dominant frequency of 63 Hz, the results are extremely close. In Fig. 9d, the discrepancy in the maximum vibration level between the two models is about 0.5 dB. Note that in the present model, the tunnel lining is represented by a shell element, whereas in the reference model, it is considered as a continuum medium. Additionally, in the present model, the ground free surface cannot be considered. These factors contributed to the discrepancies observed. In general, the present model is accurate in predicting the vibration source intensity.

On the other hand, using the 13th Gen Intel(R) Core(TM) i7-13700K 3.40 GHz CPU processor, the prediction time for the proposed model was 58 s, whereas the reference model took about 3 h. This demonstrates that the proposed model is highly efficient in terms of prediction speed.

4 Results

In this section, we examine the vibration source at the tunnel wall using the parameters outlined in Section 3. Corresponding discussion is presented in the ESM.

4.1 Vibration source with the regular slab track

Fig. 10 illustrates the effects of train speed on the vibration source intensity under soil S1 and track irregularities Q2. From Fig. 10a, the train speed will influence the vertical vibrations within 0–100 Hz, but

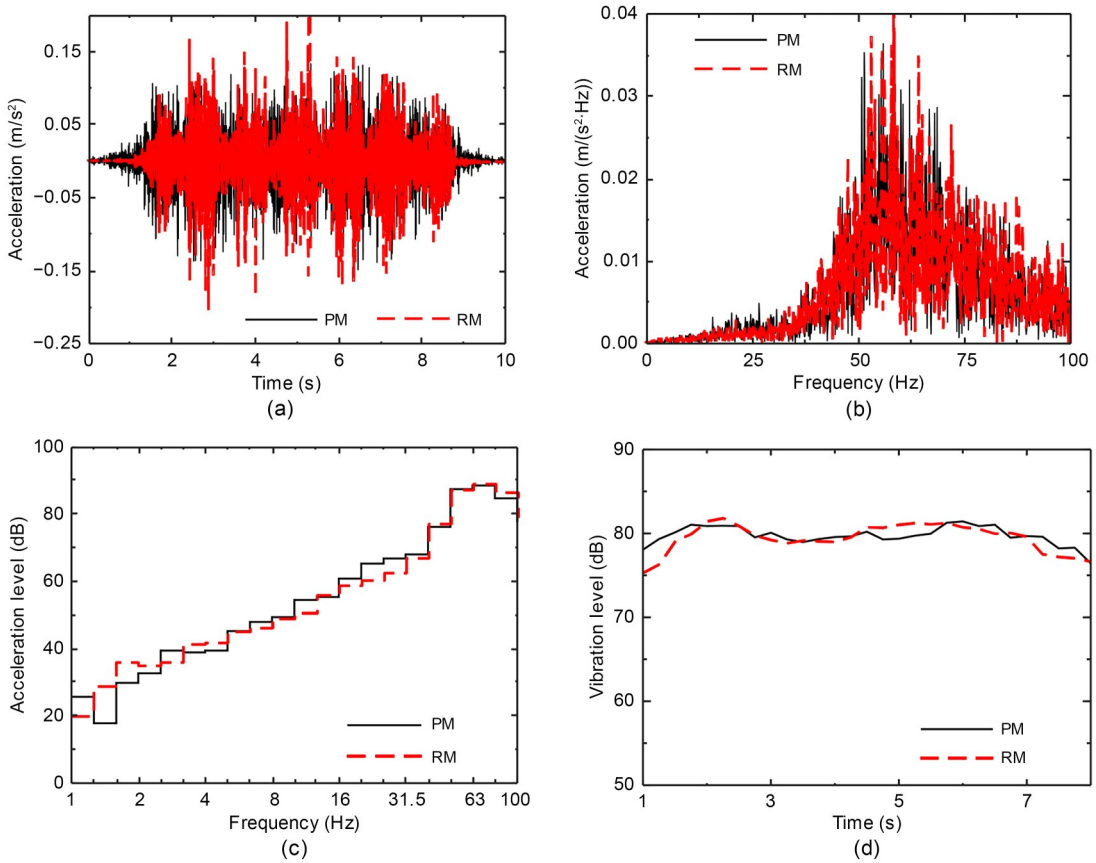

Fig. 9 Typical vibration results at the tunnel wall for v=60 km/h, S1, and Q2: (a) time history; (b) frequency spectrum; (c) one-third octave band; (d) vibration level

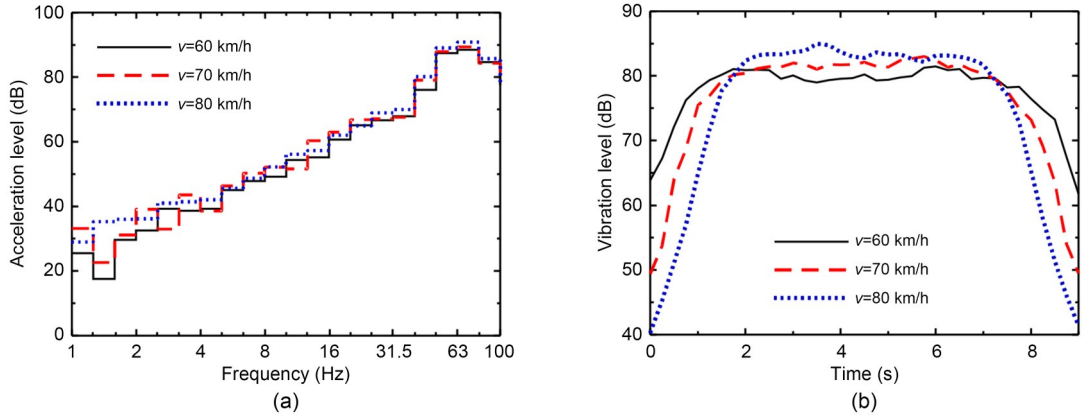

Fig. 10 Effect of train speed on vibration source intensity under S1 and Q2: (a) one-third octave band; (b) vibration level

has no impact on the dominant frequency of 63 Hz. The time history of the vertical vibration level reveals that as the train speed decreases, the duration of vibration increases and the intensity decreases. When the train speed increases from 60 to 80 km/h, the acceleration level below 100 Hz and the vertical vibration level both increase by about 3.5 dB.

Fig. 11 shows the effects of track irregularities on vibration source intensity under a train speed of v= 60 km/h and soil S1. As track conditions deteriorate from Q2 to Q4, vibrations below 100 Hz all increase, with about an 8.5-dB increase at the dominant frequency of 63 Hz, and the vibration source intensity increases by about 8.1 dB. Therefore, the vibration source intensity is

very sensitive to the track irregularities. When using comparable measurements to determine vibration source intensity, if the track conditions at the measurement section differ from those at the target section, the prediction error may be unacceptable in the environmental assessment. It is advisable to take track irregularities into account during the environmental assessment.

The effect of the surrounding soil on vibration source intensity under a train speed of v=60 km/h and track irregularities Q2 is plotted in Fig. 12. The transition from soil condition S1 to S2 results in reduced vertical vibrations within the 2–100 Hz range, with a 3.5 dB decrease at the dominant frequency of 63 Hz. The vibration source intensity decreases by about 4.2 dB. This is because when the soil is stiffer, more vibration energy transmits into the soil, resulting in less vibration energy being transmitted into the tunnel wall. The soil conditions should be considered when using comparable measurements.

4.2 Isolation effect of the floating slab track

To assess the effectiveness of the floating slab track in reducing vibrations, the concept of insertion loss, calculated as the difference between the acceleration levels of a regular track and a floating slab track, was introduced. The basic calculation parameters are v= 60 km/h, Q2, and S1. Fig. 13 illustrates the effects of train speed, track irregularities, and soil conditions on insertion loss. Below 10 Hz, the floating slab track has the potential to amplify vertical vibrations at the tunnel wall. For example, there may be an increase in acceleration levels of about 13 dB at the resonance frequency of 8 Hz. Above 10 Hz, the floating slab track demonstrates clear vibration reduction capabilities, with a maximum reduction of 34 dB at 50 Hz. Below 8 Hz, the insertion loss of the floating slab track is affected by factors such as the train speed, track irregularities, and soil conditions. Above 8 Hz, track irregularities and

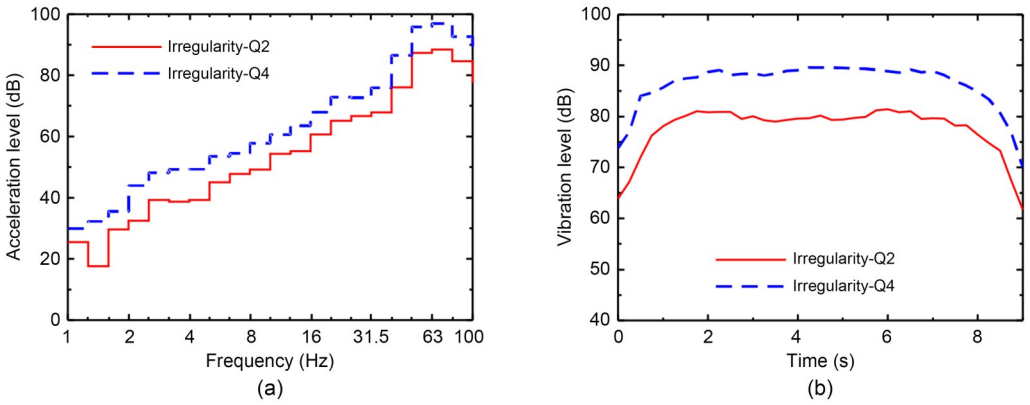

Fig. 11 Effect of track irregularities on vibration source intensity under v=60 km/h and S1: (a) one-third octave band; (b) vibration level

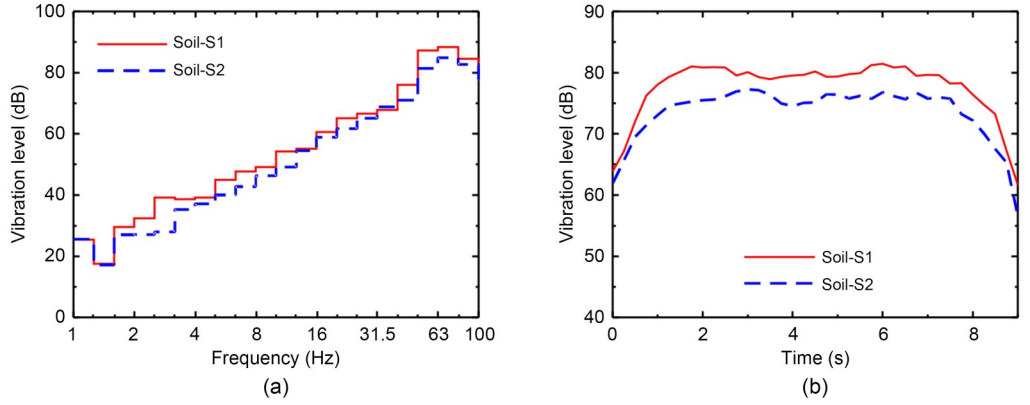

Fig. 12 Effect of soil condition on vibration source intensity under v=60 km/h and Q2: (a) one-third octave band; (b) vibration level

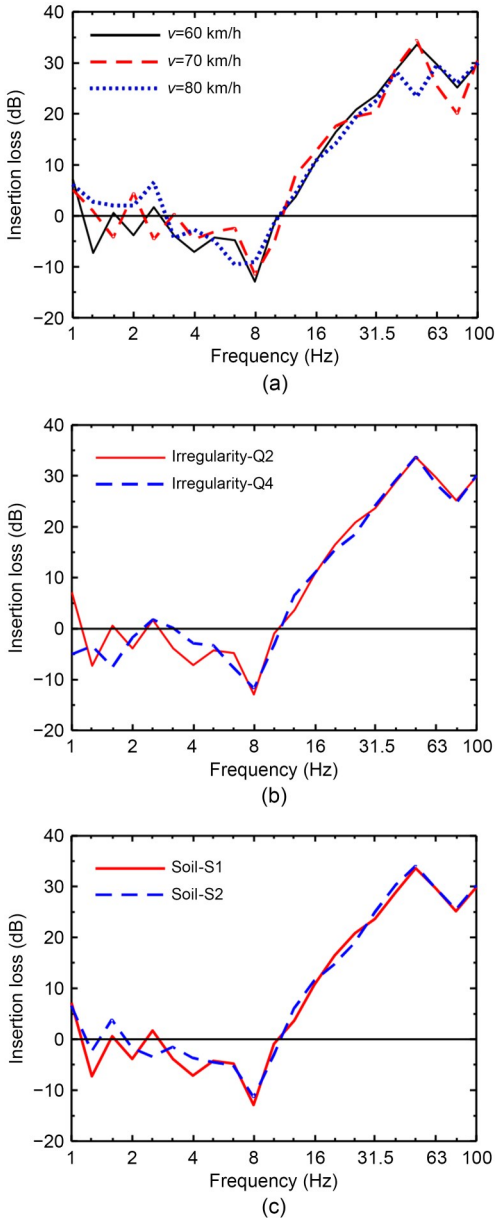

Fig. 13 Effect of train speed (a), track irregularities (b), and soil condition (c) on insertion loss of floating slab track

soil conditions have minimal impact, while the effect of train speed remains significant.

Further, Fig. 14 compares the decrease in vibration source intensity at the tunnel wall between the regular and floating slab track configurations. The reduction of vibration source intensity is about 14 dB under different cases. Given a certain train speed, the impact of soil conditions is negligible, and the greatest variation in mitigation capability across different irregularities is around 1.5 dB. As the train speed increases from 60 to 80 km/h, the vibration mitigation capability rises by 2.3 dB with track irregularities Q2 but experiences a slight decrease with track irregularities Q4. This indicates that the vibration mitigation performance of the floating slab track is affected by variables like track irregularities and train speed, with a maximum difference of about 2 dB. Using a constant vibration reduction value in the environmental evaluation will result in a prediction error of about 2 dB.

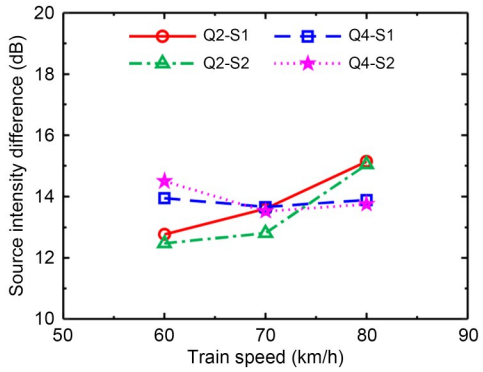

Fig. 14 Difference of vibration source intensity at the tunnel wall with regular and floating slab track

5 Conclusions

This paper presents a fast prediction method for accurately assessing the vibration source intensity caused by moving trains, considering both regular and floating slab tracks, for the empirical evaluation of environmental vibration. The PiP model is improved to incorporate the periodicity resulting from the discrete arrangement of fasteners. The regular and floating slab beams are connected to the periodic model through springs. The train load expression in the frequency-wavenumber domain is formulated. The measured track irregularities are incorporated and the accuracy and efficiency of the proposed model are confirmed. The characteristics of the vibration source under a regular slab track and the vibration isolation effects of the floating slab track are highlighted. Some conclusions are drawn as follows:

(1) The proposed method, using the periodic PiP model, is both accurate and efficient in determining the vibration source intensity. It can serve as a supplementary method alongside comparable measurements or database predictions in empirical prediction.

(2) As track conditions deteriorate from class Q2 to Q4, the vibration source intensity rises by about 8 dB.

In comparable measurements or database predictions, track irregularities must be considered a primary factor. The measured irregularities should be incorporated into the predictions.

(3) The floating slab track has a maximum vibration mitigation capacity of around 14 dB. This capability is affected by various factors, including track irregularities and train speed. Using a constant vibration reduction value in environmental assessments may lead to a prediction error of about 2 dB.

Acknowledgments

This work is supported by the Natural Science Foundation of Shandong Province of China (No. ZR2024QE071).

Author contributions

Lihui XU designed the research. Meng GAO and Xinyu TAN processed the corresponding data. Lihui XU wrote the first draft of the manuscript. Chao ZOU and Meng MA helped to organize the manuscript. Lihui XU revised and edited the final version.

Conflict of interest

Lihui XU, Meng GAO, Xinyu TAN, Chao ZOU, and Meng MA declare that they have no conflict of interest.

References

Azhir P, Asgari Marnani J, Panji M, et al., 2024. A coupled finite-boundary element method for efficient dynamic structure-soil-structure interaction modeling. *Mathematical and Computational Applications*, 29(2):24. https://doi.org/10.3390/mca29020024

Banestyrelsen, 2000. Vibrations and Structural Prediction Model, D-1115-0. BanePro 6 Rev. 1. Danmark (in Danish).

BMBMSA (Beijing Municipal Bureau of Market Supervision and Administration), 2019. Code for Metro Noise and Vibration Control, DB 11/T 838-2019. National Standards of the People's Republic of China (in Chinese).

Chen Q, 2020. Influence of Rail Wear Condition on Environmental Vibration Source Intensity Induced by Metro Trains. MS Thesis, Beijing Jiaotong University, Beijing, China (in Chinese). https://doi.org/10.26944/d.cnki.gbfju.2020.003501

Colaço A, Castanheira-Pinto A, Costa PA, et al., 2022. Combination of experimental measurements and numerical modelling for prediction of ground-borne vibrations induced by railway traffic. *Construction and Building Materials*, 343: 127928. https://doi.org/10.1016/j.conbuildmat.2022.127928

Dai F, Yang JZ, Bi LX, et al., 2024. Analysis on characteristics of ground vibration induced by underground high-speed trains based on in-situ test. *Journal of Low Frequency Noise, Vibration and Active Control*, 43(3):1097-1111. https://doi.org/10.1177/14613484241259303

Di HG, Zhou SH, Luo Z, et al., 2018. A vehicle-track-tunnel-soil model for evaluating the dynamic response of a double-line metro tunnel in a poroelastic half-space. *Computers and Geotechnics*, 101:245-263. https://doi.org/10.1016/j.compgeo.2017.12.003

Di HG, Xu PB, Gong QM, et al., 2024. Predicting ground vibrations from railway tunnels using an improved 2.5D FEM-PML model with soil spatial variability. *Engineering Computations*, 41(3):545-561. https://doi.org/10.1108/EC-06-2023-0264

Edirisinghe TL, Talbot JP, 2021. The significance of source-receiver interaction in the response of piled foundations to ground-borne vibration from underground railways. *Journal of Sound and Vibration*, 506:116178. https://doi.org/10.1016/j.jsv.2021.116178

Flügge W, 1973. Stresses in Shells. 2nd Edition. Springer, Berlin, Germany.

Forrest JA, Hunt HEM, 2006. A three-dimensional tunnel model for calculation of train-induced ground vibration. *Journal of Sound and Vibration*, 294(4-5):678-705. https://doi.org/10.1016/j.jsv.2005.12.032

François S, Schevenels M, Galvín P, et al., 2010. A 2.5D coupled FE–BE methodology for the dynamic interaction between longitudinally invariant structures and a layered halfspace. *Computer Methods in Applied Mechanics and Engineering*, 199(23-24):1536-1548. https://doi.org/10.1016/j.cma.2010.01.001

Gupta S, Hussein MFM, Degrande G, et al., 2007. A comparison of two numerical models for the prediction of vibrations from underground railway traffic. *Soil Dynamics and Earthquake Engineering*, 27(7):608-624. https://doi.org/10.1016/j.soildyn.2006.12.007

He C, Zhou SH, Di HG, et al., 2018. Analytical method for calculation of ground vibration from a tunnel embedded in a multi-layered half-space. *Computers and Geotechnics*, 99:149-164. https://doi.org/10.1016/j.compgeo.2018.03.009

He C, Zhou SH, Guo PJ, et al., 2019. A three-dimensional semi-analytical method for calculating vibrations from a moving load on a periodic jointed tunnel. *Computers and Geotechnics*, 114:103150. https://doi.org/10.1016/j.compgeo.2019.103150

He C, Jia YP, Zhou SH, 2024. Semi-analytical method for calculating ground vibrations from a tunnel in a homogeneous half-space with an irregular surface. *Journal of Sound and Vibration*, 591:118615. https://doi.org/10.1016/j.jsv.2024.118615

He YP, Peng LX, He K, et al., 2023. Analysis of uncertainty and variation in underground train-induced vibration based on measured data. *Measurement*, 222:113600. https://doi.org/10.1016/j.measurement.2023.113600

Hussein MFM, Hunt HEM, 2009. A numerical model for calculating vibration due to a harmonic moving load on a floating-slab track with discontinuous slabs in an underground railway tunnel. *Journal of Sound and Vibration*, 321(1-2):363-374. https://doi.org/10.1016/j.jsv.2008.09.023

Hussein MFM, Hunt HEM, Rikse L, et al., 2008. Using the PiP

model for fast calculation of vibration from a railway tunnel in a multi-layered half-space. Proceedings of the 9th International Workshop on Railway Noise on Noise and Vibration Mitigation for Rail Transportation Systems, p.136-142. https://doi.org/10.1007/978-3-540-74893-9_19

Hussein MFM, François S, Schevenels M, et al., 2014. The fictitious force method for efficient calculation of vibration from a tunnel embedded in a multi-layered half-space. *Journal of Sound and Vibration*, 333(25):6996-7018. https://doi.org/10.1016/j.jsv.2014.07.020

ISO (International Organization for Standardization), 2005. Mechanical Vibration-Ground-Borne Noise and Vibration Arising from Rail Systems–Part 1: General Guidance, ISO 14837-1:2005. ISO, Geneva, Switzerland.

Koopman A, Lentzen S, Steenbergen R, 2009. SRM-T: the Dutch standardized prediction model for railway vibration and induced noise. *In*: Xia H, Takemiya H (Eds.), Environmental Vibrations: Prediction, Monitoring, Mitigation and Evaluation. Science Press, Beijing, China.

Kouroussis G, Vogiatzis KE, Connolly DP, 2018. Assessment of railway ground vibration in urban area using in-situ transfer mobilities and simulated vehicle-track interaction. *International Journal of Rail Transportation*, 6(2):113-130. https://doi.org/10.1080/23248378.2017.1399093

Kuo KA, Hunt HEM, Hussein MFM, 2011. The effect of a twin tunnel on the propagation of ground-borne vibration from an underground railway. *Journal of Sound and Vibration*, 330(25):6203-6222. https://doi.org/10.1016/j.jsv.2011.07.035

Kurzweil LG, 1979. Ground-borne noise and vibration from underground rail systems. *Journal of Sound and Vibration*, 66(3):363-370. https://doi.org/10.1016/0022-460x(79)90853-8

Li MH, Ma M, Liu WN, et al., 2020. Analysis mechanism of vibration source dispersion induced by metro trains through in-situ test. *Journal of Vibration, Measurement & Diagnosis*, 40(4):738-744 (in Chinese). https://doi.org/10.16450/j.cnki.issn.1004-6801.2020.04.016

Li XT, Zhang B, Lu WC, et al., 2012. Selection of vibration source position in environment vibration forecast of Beijing metro. *Urban Mass Transit*, 15(8):80-83 (in Chinese). https://doi.org/10.3969/j.issn.1007-869X.2012.08.019

Li Z, Ma M, 2025. Probabilistic quantitative inversion of wheel out-of-roundness using probabilistic learning on manifolds and dynamic model. *Measurement*, 250:117166. https://doi.org/10.1016/j.measurement.2025.117166

Liravi H, Arcos R, Clot A, et al., 2022. A 2.5D coupled FEM–SBM methodology for soil–structure dynamic interaction problems. *Engineering Structures*, 250:113371. https://doi.org/10.1016/j.engstruct.2021.113371

Liu WF, Li CY, Ma LX, et al., 2023. A frequency-domain formulation for predicting ground-borne vibration induced by underground train on curved track. *Journal of Sound and Vibration*, 549:117578. https://doi.org/10.1016/j.jsv.2023.117578

Lu W, Yu Q, Wang L, et al., 2010. Influence of axle-load and velocity on vibration level of subway tunnel. *Noise and Vibration Control*, S1:169-171 (in Chinese).

Ma LX, 2014. Study on the Model of Coupled Vehicle & Track and the Analysis Model for Tunnel-Ground Vibration Response Based on the Periodic-Infinite Structure Theory. PhD Thesis, Beijing Jiaotong University, Beijing, China (in Chinese).

Ma M, Zhang HG, Chen Q, et al., 2021a. Effect of rail surface shortwave irregularity on metro train induced vibration source intensity. *China Railway Science*, 42(3):21-28 (in Chinese). https://doi.org/10.3969/j.issn.1001-4632.2021.03.03

Ma M, Li MH, Tan XY, et al., 2021b. Influence analysis on track vibration due to coupled irregularity excitation of metro wheel-track. *Engineering Mechanics*, 38(5):191-198 (in Chinese). https://doi.org/10.6052/j.issn.1000-4750.2020.06.0421

Ma M, Li MH, Qu XY, et al., 2022. Effect of passing metro trains on uncertainty of vibration source intensity: monitoring tests. *Measurement*, 193:110992. https://doi.org/10.1016/j.measurement.2022.110992

Ma M, Xu LH, Liu WF, et al., 2024. Semi-analytical solution of a coupled tunnel-soil periodic model with a track slab under a moving train load. *Applied Mathematical Modelling*, 128:588-608. https://doi.org/10.1016/j.apm.2024.01.038

Madshus C, Bessason B, Hårvik L, 1996. Prediction model for low frequency vibration from high speed railways on soft ground. *Journal of Sound and Vibration*, 193(1):195-203. https://doi.org/10.1006/jsvi.1996.0259

MEE (Ministry of Ecology and Environment of the People's Republic of China), 2018. Technical Guidelines for Environmental Impact Assessment-Urban Rail Transit, HJ 453-2018. National Standards of the People's Republic of China (in Chinese).

Melke J, 1988. Noise and vibration from underground railway lines: proposals for a prediction procedure. *Journal of Sound and Vibration*, 120(2):391-406. https://doi.org/10.1016/0022-460X(88)90451-8

Qu XY, Thompson D, Ma M, et al., 2023. Sources of variability in metro train-induced vibration. *Proceedings of the Institution of Mechanical Engineers, Part F: Journal of Rail and Rapid Transit*, 237(4):490-499. https://doi.org/10.1177/09544097221118456

Sheng XZ, 2019. A review on modelling ground vibrations generated by underground trains. *International Journal of Rail Transportation*, 7(4):241-261. https://doi.org/10.1080/23248378.2019.1591312

USDT (U.S. Department of Transportation), 2018. Transit Noise and Vibration Impact Assessment Manual. FTA Report No. 0123, Federal Transit Administration, Washington, USA.

Verbraken H, Degrande G, Lombaert G, et al., 2013. Benchmark Tests for Soil Properties, Including Recommendations for Standards and Guidelines. RIVAS Project SCP0-GA-2010-265754, European Union.

Vogiatzis KE, Kouroussis G, 2015. Prediction and efficient control of vibration mitigation using floating slabs: practical application at Athens metro lines 2 and 3. *International Journal of Rail Transportation*, 3(4):215-232.

https://doi.org/10.1080/23248378.2015.1076622

Xu LH, Ma M, 2020. Study of the characteristics of train-induced dynamic SIFs of tunnel lining cracks based on the modal superposition approach. *Engineering Fracture Mechanics*, 233:107069. https://doi.org/10.1016/j.engfracmech.2020.107069

Xu LH, Ma M, 2023. Analytical solution of ground-borne vibration due to a spatially periodic harmonic moving load in a tunnel embedded in layered soil. *Journal of Zhejiang University-SCIENCE A*, 24(7):637-652. https://doi.org/10.1631/jzus.A2200385

Xu LH, Ma M, 2024. Vibration amplification zone phenomenon on the ground surface under various types of buried dynamic loads within metro tunnel. *Soil Dynamics and Earthquake Engineering*, 182:108713. https://doi.org/10.1016/j.soildyn.2024.108713

Xu ZS, Ma M, Zhou ZK, et al., 2022. Prediction of metro train-induced tunnel vibrations using machine learning method. *Advances in Civil Engineering*, 2022(1):4031050. https://doi.org/10.1155/2022/4031050

Yang JJ, Li QY, Zhu SY, et al., 2024. Train-track-circular tunnel spatially coupled dynamics model and coupling effects of dynamic track-tunnel interactions. *Journal of Physics: Conference Series*, 2647(15):152005. https://doi.org/10.1088/1742-6596/2647/15/152005

Yuan ZH, Boström A, Cai YQ, 2017. Benchmark solution for vibrations from a moving point source in a tunnel embedded in a half-space. *Journal of Sound and Vibration*, 387:177-193. https://doi.org/10.1016/j.jsv.2016.10.016

Yuan ZH, Cao ZG, Tang H, et al., 2021. Analytical layer element with a circular cavity and its application in predicting ground vibrations from surface and underground moving sources. *Computers and Geotechnics*, 137:104262. https://doi.org/10.1016/j.compgeo.2021.104262

Electronic supplementary materials

Sections S1–S3